Research Article

Shujahadeen B. Aziz*, Muhamad H. Hamsan, Rebar T. Abdulwahid, Norhana Abdul Halim, Jamal Hassan*, Ahmed F. Abdulrahman, Sameerah I. Al-Saeedi, Jihad M. Hadi, Mohd F. Z. Kadir, Samir M. Hamad, and Salah R. Saeed

Green polymer electrolyte and activated charcoal-based supercapacitor for energy harvesting application: Electrochemical characteristics

https://doi.org/10.1515/gps-2023-0109
received June 24, 2023; accepted September 24, 2023

Abstract: The aim of this study is to address the growing concern about microplastics in the ocean and their potential harm to human health through ingestion. The MPs issue is largely a result of the increasing demand for electronic devices and their components. To tackle this challenge, the research aimed to develop a green polymer electrolyte that used glycerol as a plasticizing agent to improve ionic conductivity. The polymer host included chitosan and polyvinyl alcohol and was composed of sodium acetate. To evaluate the performance of the polymer electrolyte, various analytical techniques were used, including impedance and electrochemical studies. The ionic conductivity of 7.56×10^{-5} S·cm^{-1} was recorded. The dielectric property study confirmed the ionic conduction process in the system and revealed the existence of non-Debye type relaxation, as indicated by asymmetric peaks of tanδ spectra. The alternating conductivity exhibits three distinguished regions. The polymer electrolyte was discovered to be electrochemically stable up to 2.33 V and capable of storing energy as a non-Faradaic electrochemical double-layer capacitor (EDLC). The cyclic voltammetry pattern is a leaf like shape. The EDLC was able to be charged and discharged up to 1 V, and it showed cyclability and could be used in low-voltage applications.

Keywords: green electrolyte, non-toxic salt, impedance study, dielectric properties, CV and GCD study, EDLC

*** Corresponding author: Shujahadeen B. Aziz,** Hameed Majid Advanced Polymeric Materials Research Lab., Physics Department, College of Science, University of Sulaimani, Qlyasan Street, Kurdistan Regional Government, Sulaimani, 46001, Iraq; Department of Physics, College of Science, Charmo University, 46023, Chamchamal, Sulaymaniyah, Iraq, e-mail: shujahadeenaziz@gmail.com
*** Corresponding author: Jamal Hassan,** Department of Physics, Khalifa University, P.O. Box 127788, Abu Dhabi, United Arab Emirates, e-mail: jamal.hassan@ku.ac.ae
Muhamad H. Hamsan: Pusat Pengajian Citra Universiti, JalanTemuan, Universiti Kebangsaan Malaysia, 43600, Bangi, Selangor, Malaysia
Rebar T. Abdulwahid: Medical Laboratory Analysis Department, College of Health Sciences, Cihan University Sulaimaniya, Sulaimaniya, 46001, Kurdistan Region, Iraq; Department of Physics, College of Education, University of Sulaimani, Old Campus, Sulaymaniyah, 46001, Kurdistan Regional Government-Iraq
Norhana Abdul Halim: Department of Physics, Centre for Defence Foundation Studies, National Defence University of Malaysia, Sungai Besi Camp, Kuala Lumpur, 57000, Malaysia
Ahmed F. Abdulrahman: Department of Physics, Faculty of Science, University of Zakho, Kurdistan Region, Iraq
Sameerah I. Al-Saeedi: Department of Chemistry, College of Science, Princess Nourah bint Abdulrahman University, P.O.Box 84428, Riyadh, 11671, Saudi Arabia
Jihad M. Hadi: Department of Medical Laboratory of Science, College of Health Sciences, University of Human Development, Kurdistan Regional Government, Iraq
Mohd F. Z. Kadir: Department of Physics, Faculty of Science, Centre for Ionics, Universiti Malaya, 50603, Kuala Lumpur, Malaysia
Samir M. Hamad: Scientific Research Centre, Soran University, Soran, Arbīl, Kurdistan-Region, Iraq
Salah R. Saeed: Hameed Majid Advanced Polymeric Materials Research Lab., Physics Department, College of Science, University of Sulaimani, Qlyasan Street, Kurdistan Regional Government, Sulaimani, 46001, Iraq

1 Introduction

Fossil fuel consumption has caused high levels of pollution, prompting efforts to study and create renewable energy materials. Human tricks, specific energy consumption, and production are the main sources of ruthless green issues, e.g., environmental degradation and global warming [1]. Global electrical energy is 44.2% from coal, 38.0% from natural gases, 17.1% from renewable energy, and 0.6% and 5% from fuel oil/diesel and hydro, respectively. The use of coal as an energy source has a significant disadvantage in that it

emits CO_2 into the atmosphere and contributes to global warming. Natural biodegradable biopolymers, often referred to as the future "green materials," are showing great promise as ideal hosts for creating biopolymer electrolytes designed for a variety of energy devices [2,3]. These biopolymers come from sources like cellulose, starch, chitosan (CH), and alginate, and they stand out for being environmentally friendly, easy to find, and sustainable [4]. They naturally decompose over time, resulting in minimal environmental impact, representing a substantial advancement in contrast to conventional energy storage approaches; consequently, they are commonly referred to as "green" polymers [2,4]. This innovative approach not only makes energy devices like batteries, fuel cells, and supercapacitors safer and more efficient, but it also aligns with the global trend of using more sustainable resources and reducing waste. Thus, researchers are turning to green polymer membranes for electrochemical devices resembling solar cells, supercapacitors, fuel cells, and batteries to address this. This shift aims to achieve the goal of clean energy that is both sustainable and affordable [5]. Minimizing environmental impact is critical in the pursuit of a high-tech future. Micro-sized energy storage will be required for automation and robotics, which could result in a large amount of plastic waste if not properly planned for.

One of the simplest electrochemical devices is electrochemical double-layer capacitors (EDLCs) due to their simple preparation methods, long life cycles, and large power density [6,7]. In contrast to conventional batteries, EDLCs do not contain hazardous explosive components, thereby enhancing their safety profile. Moreover, the readiness of EDLCs ensures safety for both individuals and the surrounding environment. Compared to lead acid batteries, EDLC is significantly smaller and has a rapid rate of charging and discharging [8]. Carbon has been chosen as the right material to provide a large surface for ion adsorption. Electrostatic interactions between ions and electrons govern the energy storage procedure of an EDLC [9]. Activated carbon (AC) stands out as a prime candidate for EDLC electrodes due to its robust chemical and physical properties, large surface area, and porous structure [10]. Polyvinyl alcohol (PVA) is widely used to reduce plastic waste because it is a versatile polymer with properties similar to those of natural polymers, such as being eco-friendly, biodegradable, biocompatible, and having good film-forming abilities [11]. To achieve the fabrication of polymer electrolyte films with superior performance, an approach known as polymer blending can be employed, wherein additional polymers are incorporated into the polymer host. When two polymers are combined together, their functional groups will act as channels for ionic transportation [12]. It is widely recognized that polymer blends have a high concentration of functional groups, which enhances their performance in assorted fields such as drug delivery, energy storage devices (ESDs), polymer electrolytes, and tissue engineering [13]. PVA has been reported to be biocompatible with various polymers such as hydroxypropylmethylcellulose [14], dextran [15], starch [16], methylcellulose [17], and pectin [18].

CH is another excellent green polymer. CH has a linear structure made up of (1,4)-linked-2-amino-deoxy-glucan units derived via chitin deacetylation. After cellulose, chitin is the most prevalent carbohydrate on the planet [19]. CH is widely used in the green polymer edible film industry due to its film-forming properties [20]. In the food industry, CHs films are employed as bioactive packaging for the preservation of apples, raspberries, cherimoya, kiwi, and loquat [21–25]. The functional groups in the linear CH polymer chains also play a crucial role in ionic conduction, making CH a good choice for a greener future with economic and environmental benefits [26].

Glycerol is important in enhancing the performance of polymer-based electrolytes as it increases salt dissociation and ionic conductivity. This is due to glycerol's high dielectric property, which weakens the forces between cations and anions [27–29]. The addition of the right amount of glycerol boosts the ionic conductivity and mechanical strength of green polymers. In this work, a glycerol-based CH-PVA polymer electrolyte will be tested with sodium acetate (NaOAc) as the ionic source. The best performing films will be used as separator in EDLC fabrication. According to the study, incorporating green polymer electrolytes in an EDLC assembly has resulted in a breakthrough. The assembled EDLC recorded a high specific capacitance (~74 $F \cdot g^{-1}$), which is similar to values recorded for liquid and gel-based electrolytes. The electrolyte used in the EDLC assembly also displayed a relatively high energy density, comparable to that of lead-acid batteries, as illustrated in Figure 1.

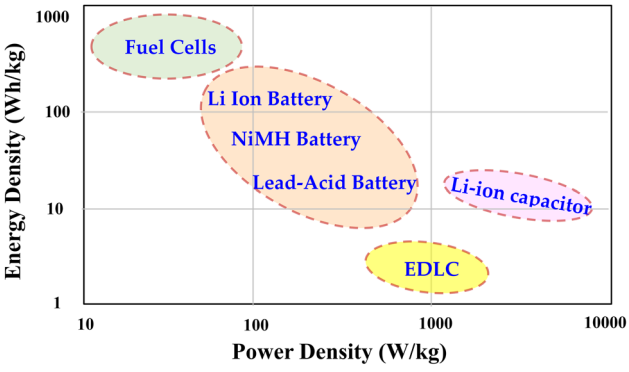

Figure 1: The Ragone plot for various electrochemical devices.

Previous research indicates that EDLC devices, which have energy densities comparable to batteries, could potentially revolutionize energy resources through the use of nontoxic materials. However, the low energy density of EDLC devices has prevented their commercialization. As a result, many research groups and companies are concentrating on developing EDLC devices with exceptionally high energy density. This would allow for novel opportunities in energy storage and expand knowledge regarding standards such as the Ragone plot for electrochemical devices. The current study's results, involving an EDLC device that delivers high energy density and excellent performance over 500 cycles, could stimulate discussion regarding the future of EDLC devices and their potential to replace battery technology. This research presents promising insights into the development of solid biopolymer electrolytes, offering potential solutions for sustainable energy storage systems.

2 Experimental method

2.1 Electrolyte preparation

CH from 75% deacetylated chitin with molecular weight [M_W : 310,000–375,000 Da, 800−2,000 cP], and PVA powder (M_W: 9,000–10,000, 80% hydrolyzed) were the polymeric materials used in the study. In this work, NaOAc (ACS reagent, ≥99.0%, M_W : 82.03) was a dopant salt, glycerol ($C_3H_8O_3$) with M_W of 92.09 g·mol^{-1}, ≥99.0%, was a plasticizer, and a mixture of deionized water and 1% acetic acid (CH_3COOH) (glacial, ≥99.7%, M_W : 60.05 g·mol^{-1}) was a solvent. All these chemicals were procured from Sigma Aldrich and employed in their as-received state without any further purification. The standard solution casting method was used to create the solid polymer electrolyte films. 0.5 g of CH and 0.5 g of PVA were dissolved in a 1% CH_3COOH solution and distilled water, respectively, at 80°C. After combining the CH and PVA solutions separately, they were blended together at room temperature for 6 h to form the CH-PVA blend solution. To create the NaOAc doped samples, 40% salt was added to the mixture. After that, we made several plasticized polymer electrolytes by adding varying quantities of glycerol to the CH-PVA-NaOAc-based polymer mix electrolyte samples. The glycerol content ranged from 11 to 55 wt% in step 11. For easy identification, the samples were labeled as CSPVNACT1, CSPVNACT2, CSPVNACT3, CSPVNACT4, and CSPVNACT5 incorporated with 11, 22, 33, 44, and 55 wt% of glycerol. Upon transferring the specimens into distinct labeled Petri dishes, they were allowed to gradually dry under ambient conditions (~30°C) and at a relative humidity of 22% for a duration of 10 days. To ensure absolute absence of moisture within the samples, further drying was employed by putting the samples in a desiccator loaded with silica gel. This careful process yielded fully dried solid polymer electrolyte (SPE) films with a thickness of 0.0278 cm, ready for characterization and the construction of an EDLC device. For accurate film thickness determination, measurements were conducted using a digital micrometer, specifically the Mitutoyo Absolute Micrometer 1D-C112XBS model.

2.2 Transference number measurement (TNM) study

The contribution of each charge carrier in an EDLC was analyzed with TNM to enhance its high performance. The analysis was conducted using a V&A Instrument DP3003 digital DC power supply. The current was recorded using a UT803 True RMS multimeter, which was connected to a computer for data extraction. The ionic (t_i) and electronic (t_e) transference numbers were determined using an equation at a voltage of 0.2 V:

$$t_i = \frac{I_b - I_{cf}}{I_b} \quad (1)$$

$$t_e = 1 - t_b \quad (2)$$

where I_{cf} and I_b are the constant flow and beginning current, respectively. In the measurement procedure, a circular segment of the most conducting CH-PVA-based SPE, was introduced between a pair of chemically inert stainless steel (SS) electrodes. These electrodes were designed with a compressed spring mechanism to ensure optimal contact. In a Teflon casing, the electrolyte sample was positioned between to SS electrodes.

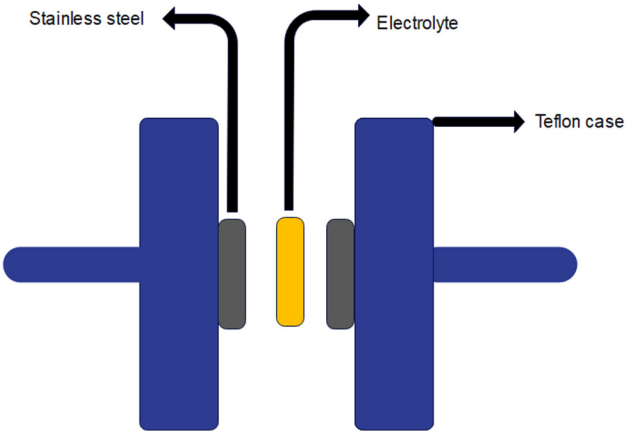

Figure 2: Schematic showing the LSV analysis electrolyte and electrode setup.

2.3 Linear sweep voltammetry (LSV) study

The ability of the SPE film as an energy storage option was evaluated using LSV. The strength, redox reactions, and behavior of the film within a range of 0–3.5 V at a sweeping rate of 50 mV·s^{-1} were examined through LSV. The investigation was completed with a Digi-IVY DY2300 Potentiostat. The top-performing CH-PVA electrolyte was positioned among two SS electrodes and enclosed in a Teflon casing for LSV analysis. The electrode and electrolyte configurations used in the LSV study, which relied solely on the most conductive electrolyte, are depicted schematically in Figure 2. This sandwich configuration allows for precise and controlled measurements of the film's electrochemical behavior and its ion transport properties in which both electrodes were constructed of SS.

2.4 Assembly of EDLC

Figure 3 depicts the methods and materials needed to create AC electrodes. A planetary ball miller was used to combine dry AC with carbon black (CB). To prevent excessive air bubble formation, the AC-CB powder was added to a solution of *N*-methyl pyrrolidone (anhydrous, 99.5%, M_W : 99.13 g·mol^{-1}) and PVdF from Merck and agitated continuously for about 5 h using a magnetic stirrer bar operating at low speed. The end product was a dark, viscous slurry that was applied over an aluminum current collector using a 0.25 mm doctor blade. The electrodes were dehydrated at 60°C for a few hours before being cooled to room temperature and placed in a desiccator to further dry. The electrodes were cut into circular forms of ~2 cm in diameter and utilized as the negative electrode in a CR2032 coin cell for testing, with the best-performing polymer electrolyte sheet sandwiched between the two electrodes. Within this investigation, AC serves as the electrode substance due to its chemical durability, exceptional conductivity, substantial specific surface area exceeding 2,000 m^2·g^{-1}, and notable porosity.

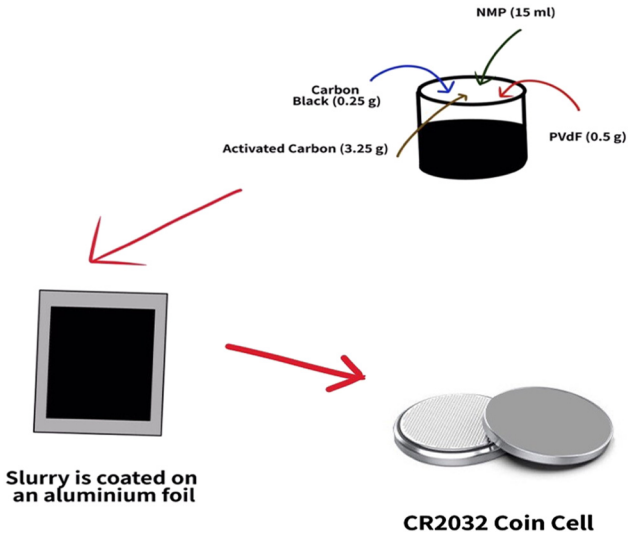

Figure 3: The fabrication process of the EDLC.

2.5 Device characterizations

2.5.1 Cyclic voltammetry (CV) study

The method of charge storage in EDLC is based on capacitive charge separation, as opposed to redox reactions. To affirm this mechanism, the EDLC was subjected to a CV study. The capacitance (C_{cyc}) was tracked as the scan rate was incrementally adjusted from 10 to 100 mV·s^{-1}. The C_{cyc} was computed using the following mathematical expression:

$$C_{cyc} = \frac{\int_{V_i}^{V_f} I(V)\mathrm{d}V}{2mx(V_f - V_i)} \tag{3}$$

The CV plot area, $I(V)\mathrm{d}V$, was calculated using Origin 9.0 software with the integration function. The starting and ending potentials (V_i and V_f) were set as 0 and 1 V, respectively, with "*m*" representing the mass of AC and "*x*" representing the scan rate.

2.5.2 Galvanostatic charge–discharge (GCD) of assembled EDLC

The GCD test was conducted using a 1.4 mA·cm^{-2} current density and a NEWARE battery cycler. The key EDLC parameters counting, specific capacitance (C_s), energy and power densities (E and P), equivalent series resistance (ESR), and efficiency (η) were the focus of this research:

$$C_s = \frac{i}{sm} \tag{4}$$

$$\mathrm{ESR} = \frac{V_{dr}}{i} \tag{5}$$

$$E = \frac{C_s V^2}{2} \tag{6}$$

$$P = \frac{V^2}{4m\mathrm{ESR}} \tag{7}$$

$$\eta = \frac{t_d}{t_c} \times 100\% \tag{8}$$

where the symbol "s" stands for the decline in the discharge region, "V_{dr}" denotes the decrease in potential, and "*i*" represents the current density in operation.

3 Result and discussion

3.1 EIS and AC conductivity study

The characterization of ionic conductivity in polymeric materials can be effectively carried out through the use of electrochemical impedance spectroscopy [30]. This technique allows for the determination of inter-particle interactions, including grain and grain boundary effects, through the analysis of complex impedance data [31]. Figure 4 displays the Cole–Cole plot for the plasticized systems to determine the DC conductivity. Typically, the frequency domain analysis of impedance spectra yields two distinct regions, a half-circle at high frequency and a line at low frequency. It has been suggested that the low-frequency (LFr) line arises from the contribution of blocking electrodes, while the high-frequency (HFr) half-circle reflects the ionic conduction mechanism of the bulk electrolyte [32–34]. The interface between electrodes and electrolyte samples can be viewed as a capacitor in the presence of blocking electrodes. When the impedance is ideal, the impedance plot displays a vertical spike. It is notable that an increase in plasticizer concentration is known to result in a decline in the HFr semicircle diameter [35]. Each sample's bulk resistance (R_b) is shown in the insets of the impedance charts. The equation given below indicates that the DC ionic conductivity in polymer-based electrolytes is linked to the ion density and mobility [36]:

$$\sigma = \sum nq\mu \tag{9}$$

where n, q, and μ denote the total number of ions, charge of ions, and ionic mobility, respectively. According to the formula, increasing either ion mobility or charge carrier density results in improved DC ionic conductivity. By following up on impedance plots and locating the real axis value at the semicircle's lowest point, one may estimate the dc value. Following is an equation that could be used to compute the DC conductivity:

$$\sigma_{dc} = \left(\frac{1}{R_b}\right) \times \left(\frac{t}{A}\right) \tag{10}$$

where A and t represent the area and thickness of the sample, respectively [37]. Table 1 lists the DC conductivity of the polymer electrolytes (PEs) in which the conductivity boosts with glycerol incorporation as the glycerol improves more mobile ions into the PE and decreases the R_b. The reduction in R_b leading to its minimum value corresponds to the attainment of the highest conductivity (7.56×10^{-5} S·cm^{-1}), indicating the successful interaction among the components of the electrolyte. The LFr spike appearance in Figure 4(b–e) indicates dissociation of more salts by glycerol and thus increase in conductivity. This is attributed to the improved flexibility of the polymer chains, which helps in faster migration of ions.

3.2 AC conductivity

In Figure 5, the frequency dependency of the AC conductivity in the CH-PVA-NaOAc-glycerol systems is demonstrated. Conductance spectra typically exhibit three regions: an LFr zone due to a proper electrode polarization (EP), a plateau region representing the DC conductivity of the system, and an HFr zone due to bulk structural interactions. Determining AC conductivity in disordered materials can be a complex task due to the diverse range of charge states that are present [38–40].

The frequency behavior provides a valuable tool for evaluating the localization of states. A remarkable conductivity dispersion is a hallmark of electrical conduction in disordered materials, often described as a combination of a frequency-independent term and a frequency-dependent contribution [39]. The equation below summarizes this relationship:

$$\sigma_{(\omega)} = \sigma_{ac} + \sigma_{dc} \tag{11}$$

where $\sigma(\omega)$ signifies the total conductivity, and σ_{ac} and σ_{dc} denote the frequency-dependent AC conductivity and frequency-independent DC conductivity, respectively. The alternating current conductivity is given by the expression ($A\omega^S$), where A is a temperature-dependent parameter, and ω is a power law exponent. This research showed that the doped systems had two distinct regions: an LFr dispersion zone originated by ion-blocking at the electrode–electrolyte interface, and a plateau mid-frequency area that reflects bulk conductivity [39]. The DC conductivity, extrapolated from the plateau area to zero frequency, was found to be in agreement with the Cole–Cole plotted values. At low frequencies, the conductance was observed to be high due to the buildup of charges at the electrodes, while at intermediate frequencies, low applied field duration and a gradual charging procedure led to an AC conductivity value similar to DC conduction [38–40].

3.3 Dielectric properties

The complex dielectric permittivity (ε) of materials is given as $\varepsilon = \varepsilon' + j\varepsilon''$. Figures 6 and 7 demonstrate the variation in ε' and ε'' parameters alongside frequency, correspondingly. The ε' represents the charge storages, whereas ε'' represents the amount of energy lost during movement of ions [41,42]. The ε' and ε'' were retrieved from the real and imaginary sections of complex impedance spectroscopy using the formulae given below:

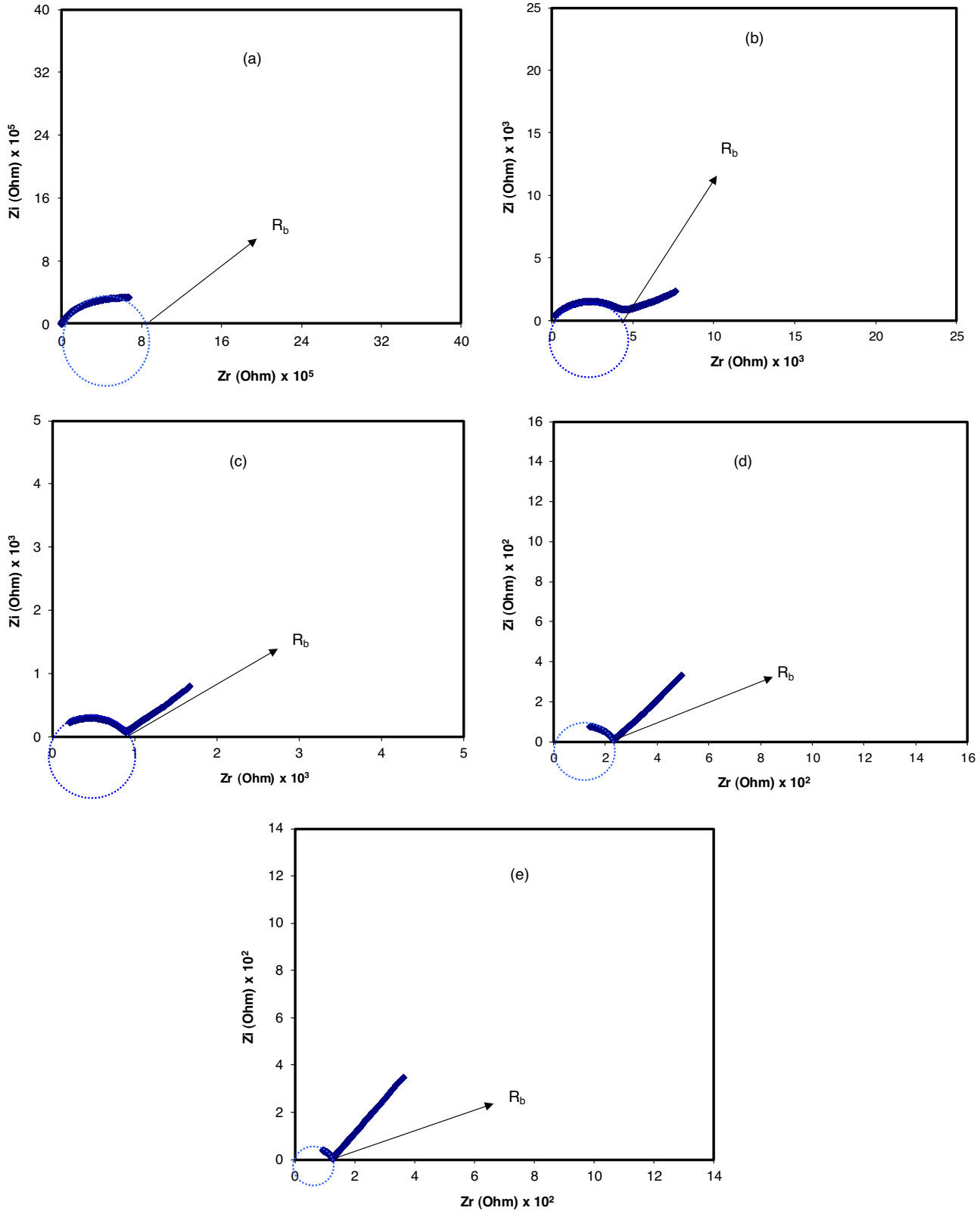

Figure 4: Cole–Cole plot for the plasticized systems (a) CSPVNACT1, (b) CSPVNACT2, (c) CSPVNACT3, (d) CSPVNACT4, and (e) CSPVNACT5 to determine the DC conductivity.

Table 1: DC ionic conductivity of the CSPVNACT samples

Sample code	DC conductivity (S·cm^{-1})
CSPVNACT1	9.85×10^{-9}
CSPVNACT2	2.27×10^{-6}
CSPVNACT3	9.84×10^{-6}
CSPVNACT4	3.85×10^{-5}
CSPVNACT5	7.56×10^{-5}

$$\varepsilon' = \frac{Z_i}{\omega C_o (Z_r^2 + Z_i^2)} \tag{12}$$

$$\varepsilon'' = \frac{Z_r}{\omega C_o (Z_r^2 + Z_i^2)} \tag{13}$$

The symbol C_o represents vacuum capacitance, $\omega = 2\pi f$ indicates the angular frequency, and f represents the working frequency. At low frequencies, EP at the electrode surface causes a dispersion region to appear. Meanwhile, high frequencies exhibit a plateau region due to the ionic dipoles' inability [41,42]. The connection among the dielectric constant and the quantity of free ions in the electrolytes is as follows:

$$n = n_o e^{\frac{-U}{\varepsilon' k_B T}} \tag{14}$$

where U displays the dissociation of energy, k_B is the Boltzmann constant, and n_o denotes the pre-exponential factor. Figure 6 shows how the ε' readings improved after the increment in glycerol concentrations. The system with 55 wt% glycerol shows the best ε' value, indicating the largest number of free ions in the system. This result is consistent with the EIS and AC conductivity results. In the study, the dielectric constant has a lower value than the dielectric loss, indicating that the movement of the carriers contributes to the dielectric loss value [43–45]. The high ε'' value at LFr is due to the mobility of the free charges inside the material. These values do not accurately represent the intrinsic bulk dielectric characteristics of the material, primarily due to the accumulation of free charges at the interface between the electrodes and the electrolyte. At LFr, there is enough time for charges to collect at the interfaces prior to the reversed dielectric field, leading to a noticeable high rate of ε'. However, at HFr, there is no enough time for charges to store at the boundary, but only polarize at the bulk of the materials. This results in conductivity relaxation [46]. Additionally, at LFr zones, ions and dipoles have enough time to bring into line themselves in the trend of the applied electric field. As a result, the aggregation of charge carriers at the boundary produces EP, which decreases the HFr dielectric characteristics (bulk properties) [47].

Ionic conductivity in polymer electrolytes is a multifaceted process affected by salt concentration and dissociation, polymeric host dielectric characteristics, chain flexibility, and ion aggregation [44,48]. A key feature of ion-conducting polymer electrolytes is their ionic conductivity; the dielectric study of these systems is also of great importance in gaining an understanding of ion transport and ion-molecule

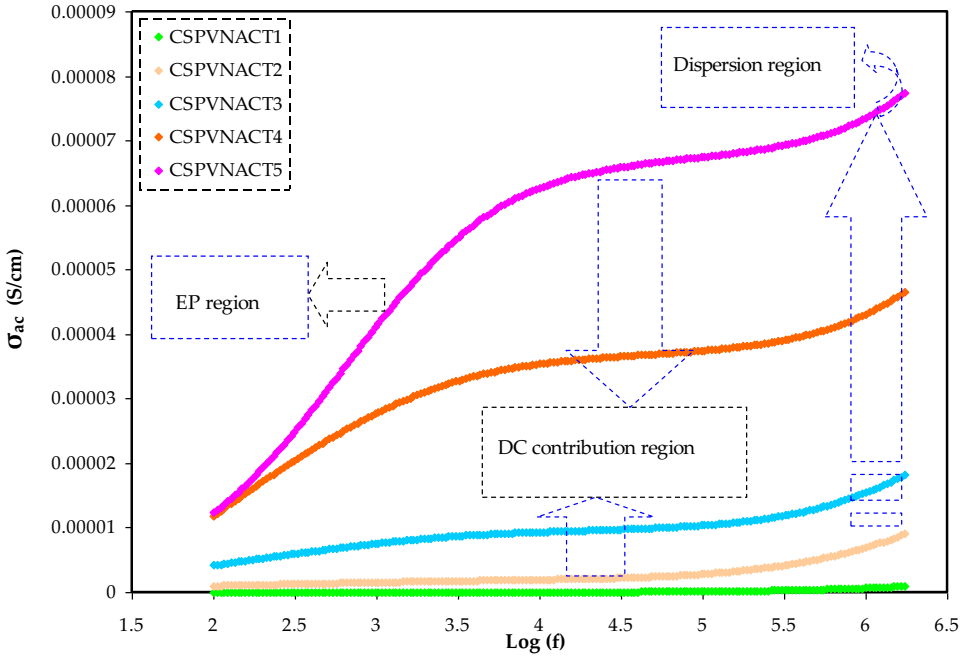

Figure 5: AC conductivity plot for the plasticized systems to distinguish EP, DC, and dispersion regions.

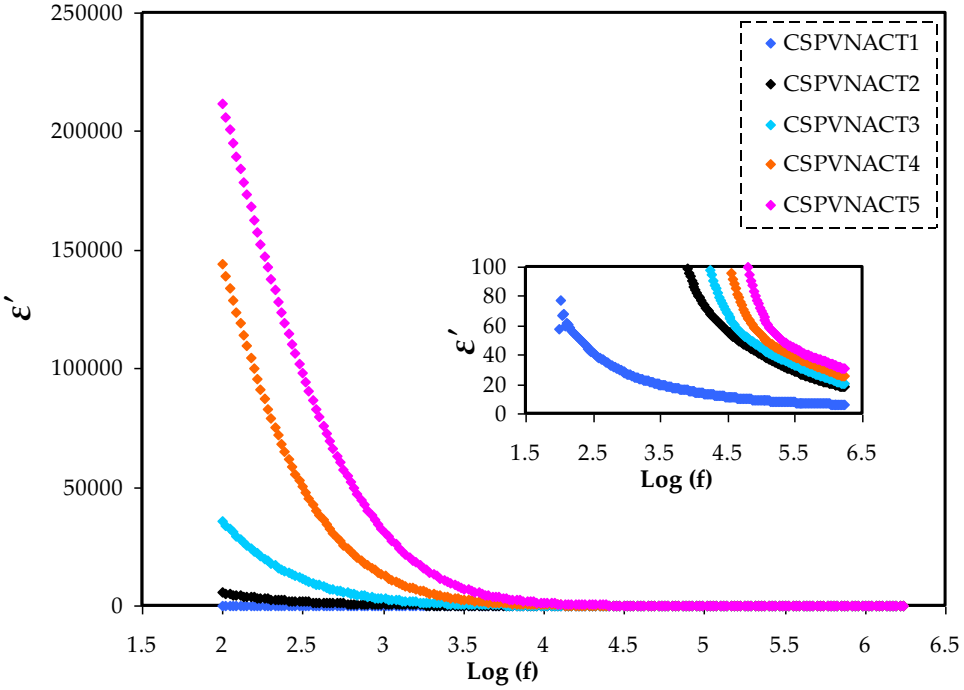

Figure 6: The variation in ε' against frequency for the CSPVNACT samples.

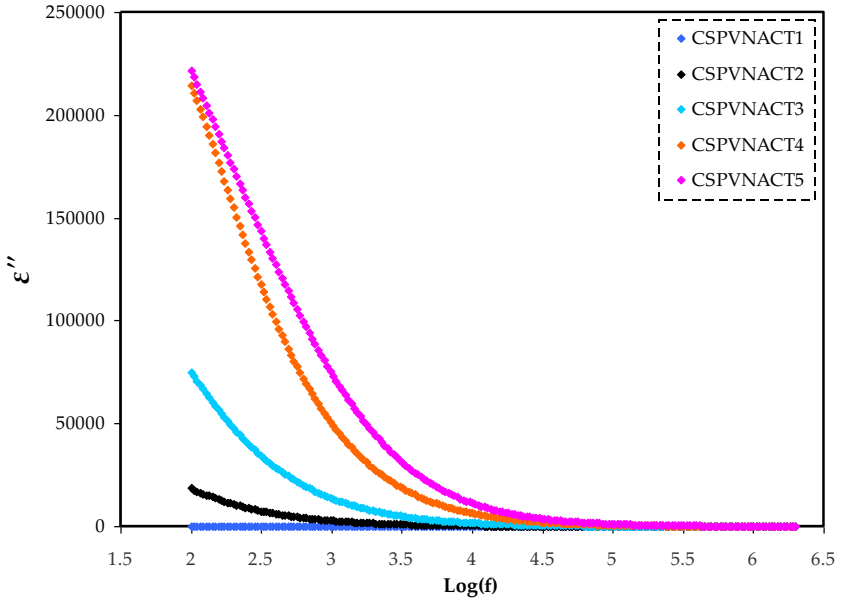

Figure 7: The variation in ε'' against frequency for the CSPVNACT samples.

interactions in solid polymer electrolytes [49]. Figure 8 shows the variation in loss tangent (tanδ) against frequency for the CSPVNACT electrolytes. It can be seen that the loss tangent peaks of the CSPVNACT samples change in frequency as a function of the plasticizer concentration. The relaxation peaks observed in the plasticized electrolytes could be attributed to almost complete ion relaxation times. The presence of a relaxation process in the CSPVNACT samples signifies that glycerol enhances the segmental motion of the polymer blend chains, consequently promoting increased free volume and improved ion transport [50,51]. Quick segmental motion and ionic mobility both contribute to ionic transport within the CH-PVA blending matrix. Table 2 shows the relaxation time values extracted from

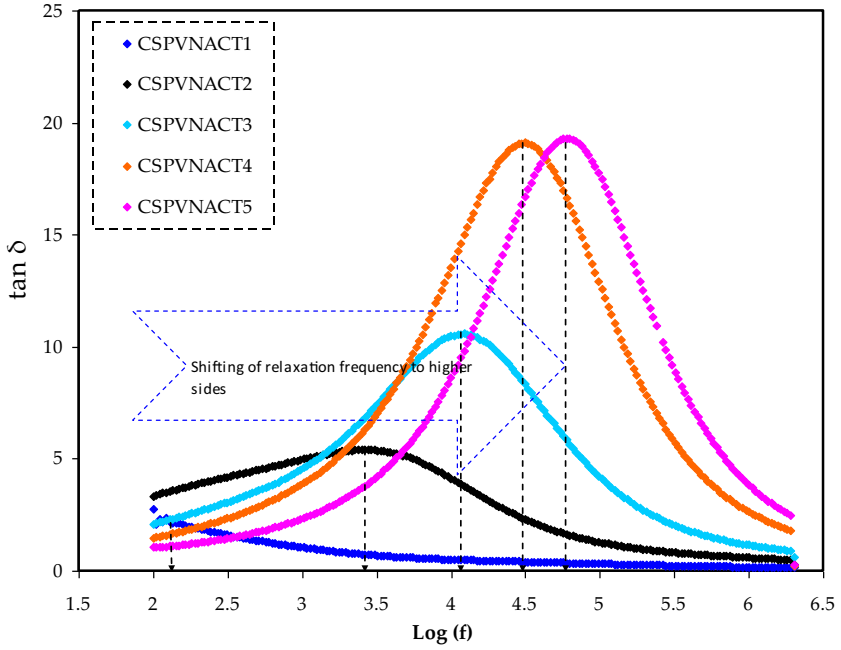

Figure 8: Tanδ vs Log(f) for all CSPVNACT electrolytes.

frequency peaks. It shows that adding plasticizers via salt dissociation could enhance carrier concentration and segmental motion and thus reduce the required time for DC conduction [52]. The peak shifts to the HFr side, demonstrating the shorter relaxation period. The outcomes of the present investigation are in line with those reported in prior studies [53]. The dielectric field and polarization are in phase at low frequencies, while the polarization lags behind the electric field frequency at high frequencies. The dielectric loses energy and emits heat as a consequence of the phase change. When the relaxation process is equal to the duration of the applied electric field, maximum loss tangent is obtained, resulting in a resonant state [54]. According to Jiang et al. [55], the principal reason of the rise in the loss tangent (tanδ) with increasing frequency of operation is resistive losses. This phenomenon arises due to the challenge faced by the ionic mobility of the electrolyte samples in keeping pace with HFr electric fields. As can be seen in Figure 8, the tanδ value increases with frequency, climbs to its maximum value, and then declines. Moreover, the highest loss tangent value shifts to high frequency along with an increase in glycerol concentration.

3.4 Electrochemical studies

3.4.1 LSV study

The LSV is used to determine the breakdown voltage of polymer electrolyte membranes. The application of voltage will reveal any redox reactions within the polymer electrolyte. Figure 9 presents the breakdown voltage profile of the CH-PVA electrolyte film, which demonstrates exceptional stability. No significant current is observed as the film is subjected to a linear potential sweep from 0 to +2.33 V. This represents the creation of a charge double-layer (CDL) at the interface of the polymer electrolyte and SS electrodes. When the potential exceeds 2.33 V, the current value sharply increases. The plot established that the CH-PVA film has decomposed beyond +2.33 V, which indicates the degradation of oxide or oxidation of functional groups [56]. This phenomenon triggers the polarization process to be unstable. This is a general idea that the performance of the EDLC will be unstable at potentials greater than 2.33 V. As reported by Vahini et al. [57], the Na-based polymer electrolyte film exhibited instability in its current response when the applied potential exceeded 2 V. A study indicated that a polymer electrolyte incorporating sodium iodide (NaI) as the ionic source and methylcellulose as the polymer host demonstrated electrochemical stability up to

Table 2: Relaxation time extracted from peak frequency

f	$T = 1/(2\pi f)$
105	1.51×10^{-3}
2,050	7.77×10^{-5}
13,460	1.18×10^{-5}
26,920	5.92×10^{-6}
51,244	3.11×10^{-6}

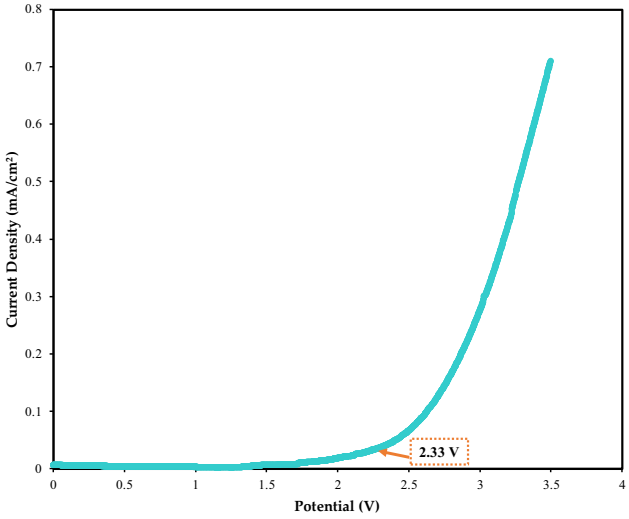

Figure 9: The LSV plot at 50 mV·s^{-1} for the best conducting polymer electrolyte.

1.7 V [58]. Hence, the optimized CH-PVA electrolyte in this work can be useful in low voltage energy storage applications.

3.4.2 Transference number study

Most ESDs rely on the ionic species of the polymer electrolyte. Ions are required in an EDLC to ensure that the energy storage process can be done via the CDL. TNM analysis is one of the easiest ways to check the dominance of a charge carrier. Figure 10 presents the TNM plot of the most conducting CH-PVA film at 0.2 V driving voltage. Both electrons and ions were thought to contribute equally to the current, hence 6.3 µA was the first value used for I_b. But it was not long until the current value dropped dramatically, leveling out at a constant 1 µA. Small, steady current flow shows that the SS electrodes are successfully inhibiting ion flow. When a certain voltage is applied to the electrolyte, both anions and cations flow toward their respective electrodes, where a CDL develops on the electrodes' surfaces, through which only electrons may pass [59,60]. Based on the outcome, it is verified that polarization, which is important for an EDLC, is possible in CH-PVA electrolyte. Ions have been established as the principal charge carriers governing the overall conduction, attributed to the elevated concentration of t_i (0.84). Polyethylene oxide-sodium thiocyanate (NaSCN) electrolyte is reported to have a t_i of 0.89 [61]. Ibrahim et al. [62] reported a polyurethane-NaI system with a t_i of more than 0.8. As the inclusion of sodium fluoride (NaF) increased from 6 to 10 wt%, the t_i of PVA-polyvinylpyrrolidone film increased from 0.89 to 0.909 [63].

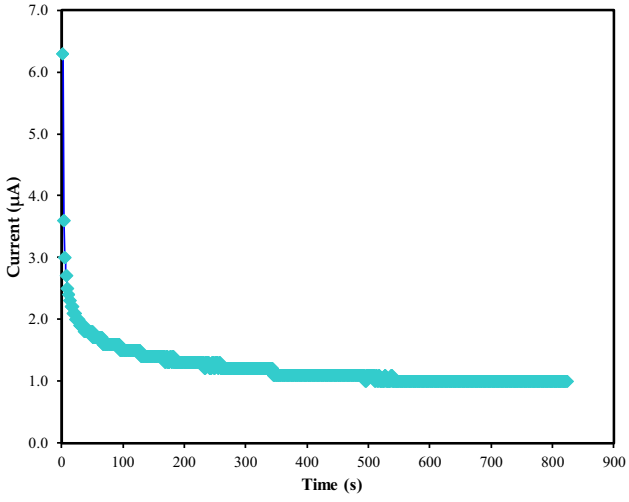

Figure 10: The TNM plot for the optimal conducting polymer electrolyte.

3.4.3 CV of the assembled EDLC

The electrostatic interactions between the electrons of the carbon-based electrodes and the ions of the electrolyte

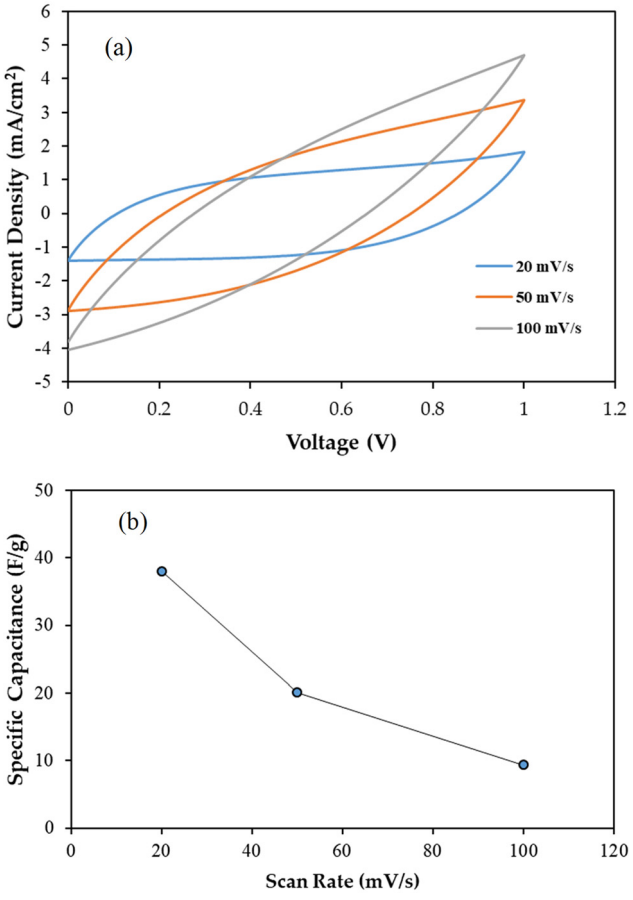

Figure 11: (a) CV curves of the CH-PVA based EDLC at various scan rates and (b) specific capacitance as opposed to scan rate.

cause the energy storage, which is known as a non-Faradaic capacitor. Through CV analysis, the existence of non-Faradaic processes in the EDLC was verified. The CV curve when the scan rate was lowered from 100 to 20 mV·s^{-1} is shown in Figure 11(a) and (b) displays the specific capacitance as opposed to scan rate. As observed in Figure 11(a), the CV curve of the EDLC at 100 mV·s^{-1} looks like the shape of a typical leaf, where the calculated C_{cyc} is 9.4 F·g^{-1}. At a rapid scan rate, the development of the CDL is unstable due to the imbalance conduction of ions [64]. As the scan rate decreased to 50 and 20 mV·s^{-1}, the C_{cyc} is obtained as 20 and 38 F·g^{-1}, respectively. The curve at the edges of the plot of 20 mV·s^{-1} is smaller than 50 and 100 mV·s^{-1}. Furthermore, the plot has deviated to a rectangular-like shape at 20 mV·s^{-1}. This indicates a low internal resistance. The efficient and stable transport of ions occurs at a low current flow, allowing complete polarization of ions. Figure 12 shows the schematic design of the fabricated EDLC. Obtaining a perfect rectangular shape CV plot is challenging due to the roughness of the carbon electrodes, as their porosity causes a varying distance between ions in the electrolyte and their corresponding active sites in the AC electrode. Figure 13 shows the mechanism of CDL formation in EDLC. The absence of humps or peaks in the plot confirms that the EDLC in this work functions as a non-Faradaic capacitor, exhibiting the scan rate-dependent characteristics typical of capacitor cells.

3.4.4 Charge–discharge of the assembled EDLC

The charge–discharge curve for the EDLC is displayed in Figure 14 for a number of cycles. The EDLC is charged to a maximum of 1 V and then discharged down to 0 V. Because of the electrostatic interaction between the ions in the electrolyte and the electrons in the electrodes, the curve should normally have a triangular form. However, because of the intercalation and de-intercalation processes, the discharge curve for ordinary batteries is often non-linear [65].

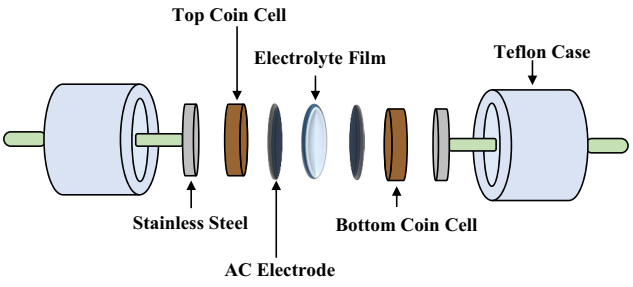

Figure 12: Schematic illustration of EDLC setup.

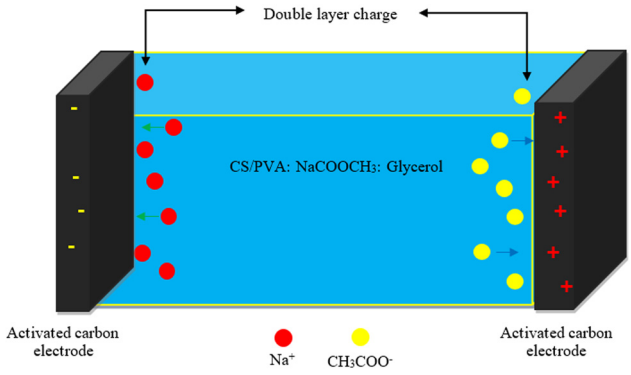

Figure 13: Mechanism of CDL formation in EDLC.

Figure 15 shows the CH-PVA-based EDLC's capacitance (C_s) and efficiency when the current density is 1.4 mA·cm^{-2} as a function of the cycle number. The C_s values remain almost constant, with an average of 77 F·g^{-1}. When the sample material is placed between the electrodes, the charge carriers move through the polymer electrolyte film and form the EDLC. This results in ion polarization stabilization and charge accumulation on both electrodes. The efficiency of an EDLC is considered high if its discharge time is close to or greater than its charge time. The initial cycle had an efficiency of 71.3%. Initially, charging usually takes longer than discharging, until stability is reached. However, after the 50th cycle, the efficiency remains consistently high, ranging between 99% and 100%. This result shows that the EDLC has exceptional stability over multiple cycles [66–68].

The ESR is a crucial factor for determining the quality of the electrolyte–electrode interface and the internal resistance of an EDLC. Figure 14 shows a noticeable voltage drop (V_{dr}) before the discharge process. The EDLC's average V_{dr} was around 0.12 V. Figure 16 depicts the EDLC's ESR values across 500 complete charge–discharge cycles with an average value of 87 Ohms. This is due to the polymer electrolyte and the gap

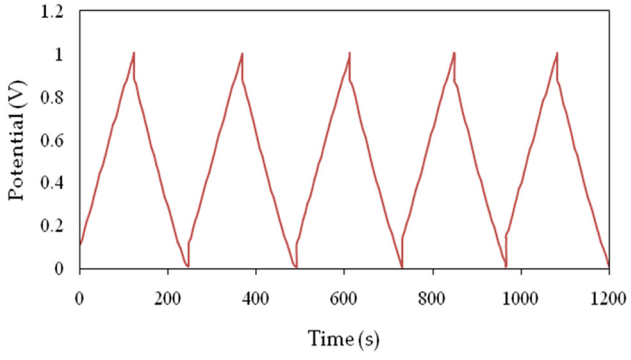

Figure 14: The GCD for the EDLC device.

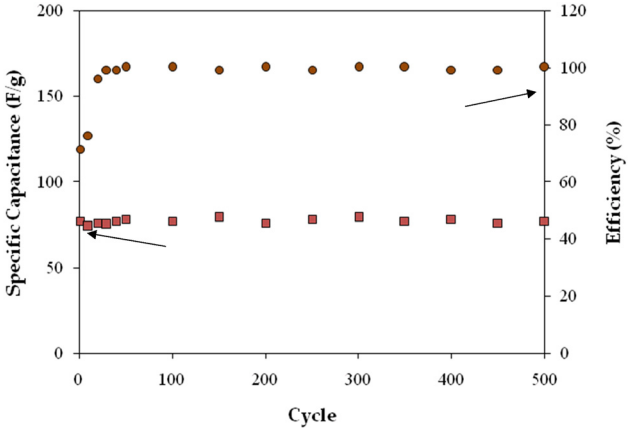

Figure 15: Calculating the EDLC's efficiency over 500 cycles and its specific capacitance.

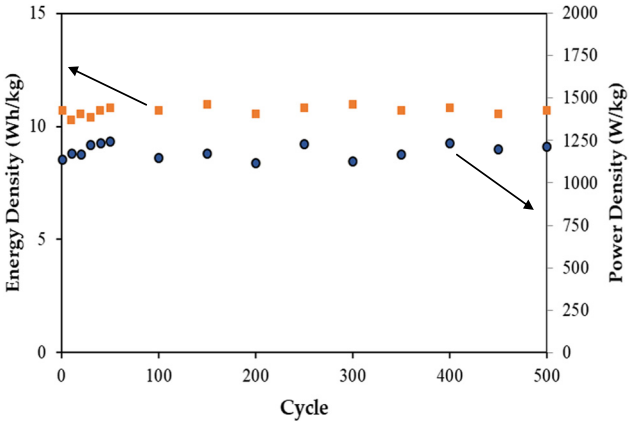

Figure 17: The *E* and *P* of the assembled EDLC.

between the electrodes and the electrolyte in the EDLC [66]. Lower ESR values indicate a good connection between the electrodes and the electrolyte, allowing for efficient charge carrier conduction to the electrodes and the formation of a CDL through electrostatic interactions [69].

Figure 17 illustrates the changes in *E* and *P* in the constructed EDLC throughout 500 cycles. The stored energy begins at 10.6 $Wh{\cdot}kg^{-1}$ during the first cycle and ultimately stabilizes at 10.7 $Wh{\cdot}kg^{-1}$. Because of comparable energy barriers, the mobile ions in the CH-PVA polymer matrix may readily migrate toward the electrodes [70]. EDLCs built of biopolymers, according to Winie et al. [71], may have energy densities varying from 0.57 to 2.8 $Wh{\cdot}kg^{-1}$, depending on the change in current density from 2 to 0.6 $mA{\cdot}cm^{-2}$. The stability of energy density and capacitance patterns suggests that ionic aggregation is unlikely. At the beginning of the first cycle, the *P* value is 1,139 $W{\cdot}kg^{-1}$ and swings somewhat, with an average *P* of 1,188 $W{\cdot}kg^{-1}$. Because charge transfer is connected with the gap between the electrolyte and electrodes, *P* has a high association with ESR [72].

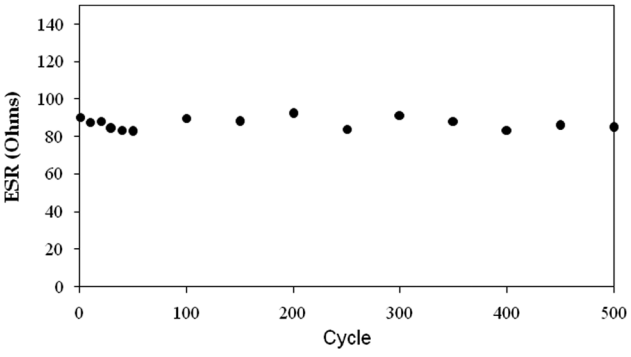

Figure 16: ESR plot of the assembled CH-PVA based EDLC throughout the 500 cycles.

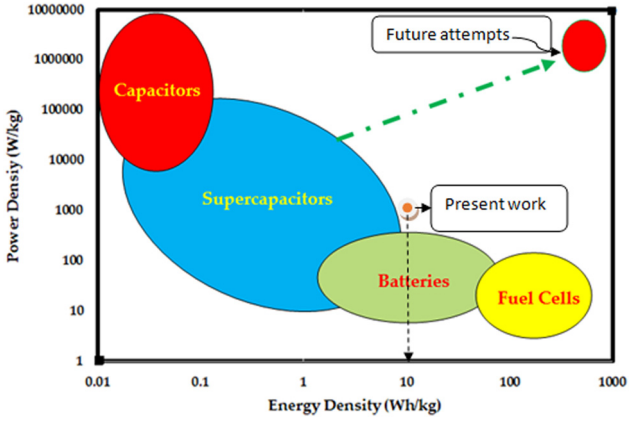

Figure 18: The obtained energy density position in Ragone plot.

ESDs need to store a lot of energy and provide quick access to electricity when needed. To compare different ESDs, scientists use the Ragone plot, which shows the relationship between energy density ($Wh{\cdot}kg^{-1}$) and power density ($W{\cdot}kg^{-1}$) on a logarithmic scale. Examples of ESDs include batteries, capacitors, supercapacitors, flywheels, and magnetic ESDs, which occupy different regions on the Ragone plot. When choosing an ESD, power density is an important factor to consider. The study suggests that EDLC devices based on biopolymers are the future of energy storage, but more research is needed to ensure consistent results. To achieve this, researchers need to carefully prepare films, encapsulate the ESDs properly, and analyze the results thoroughly. Our group is working on developing EDLC ESDs that are as good as or better than batteries. To our knowledge, EDLC is the future of ESDs, provided that it can store energy like a battery. The goal for EDLC in the future is shown in Figure 18, and achieving it will help protect us from toxic materials and reduce the effects of temperature changes on our environment.

4 Conclusion

A polymer blend electrolyte composed of CH, PVA, NaOAc, and glycerol has been created as a means of reducing plastic waste, particularly micro-plastics, in oceans. This material was found to be suitable for use as an electrode separator in an AC-based EDLC. It was found that at 55% glycerol, the system revealed a high ionic conductivity of 7.56×10^{-5} S·cm^{-1}. The dielectric property study confirmed the ionic conduction process in the system and revealed the existence of non-Debye type relaxation, as indicated by asymmetric peaks of the loss tangent pattern. The alternating conductivity exhibits EP, a plateau (mid frequency region) and dispersion region at high frequency. The majority of the conductivity in the electrolyte was due to ions, with a contribution of 0.84, while electrons contributed only 0.16. The highest conducting CH-PVA-NaOAc-glycerol electrolyte has a potential limit of 2.33 V and can be applied in various electrochemical applications. With no redox peaks in the CV plot and a scan rate-dependent capacitance of 9.4–38 F·g^{-1}, it was clear that the EDLC exhibited capacitive behavior. In the future, the use of other plasticizers such as sorbitol and polyethylene glycol could increase the salt dissociation and improve the specific capacitance of the electrolyte. Additionally, replacing NaOAc with a salt with lower lattice energy may also increase the conductivity value. The charge and discharge measurement of the CH-PVA-NaOAc-glycerol-based EDLC showed an average specific capacitance of 77 F·g^{-1}, an ESR of 87 Ohms, an energy density of 10.7 Wh·kg^{-1}, and a power density of 1,188 W·kg^{-1}. The EDLC also demonstrated high cycling ability by completing 500 charge–discharge cycles. The performance of the EDLC, can be improved by incorporating nano-fillers, polymer grafting, and utilizing different types of carbon, salt, and polymers to enhance both electrodes and electrolytes, which are key components of EDLC. Ensuring tight contact between the electrodes and electrolytes is crucial in achieving this improvement. In conclusion, microbial-based EDLC has proven to be a viable option for low-voltage applications.

Acknowledgements: The authors gratefully acknowledge all supports for this study from the Ministry of Higher Education and Scientific Research-Kurdish National Research Council (KNRC), Kurdistan Regional Government. The financial support from the University of Sulaimani, and University of Human Development and University of Cihan Sulaimaniya are greatly appreciated. This research is partially funded by Khalifa University fund number CIRA-2020-051. The authors express their gratitude to the support of Princess Nourah bint Abdulrahman University Researchers Supporting Project number (PNURSP2023R58), Princess Nourah bint Abdulrahman University, Riyadh, Saudi Arabia.

Funding information: Authors state no funding involved.

Author contributions: Shujahadeen B. Aziz, Muhamad H. Hamsan, and Rebar T. Abdulwahid: formal analysis, methodology, investigation, and writing original draft; Shujahadeen B. Aziz, Norhana Abdul Halim, Jamal Hassan, Mohd F. Z. Kadir, and Salah R. Saeed: conceptualization, supervision, project administration, and writing – review and editing; Ahmed F. Abdulrahman, Sameerah I. Al-Saeedi, Jihad M. Hadi, and Samir M. Hamad: validation, funding acquisition, and writing – review and editing.

Conflict of interest: Authors state no conflict of interest.

Data availability statement: The datasets generated during and/or analyzed during the current study are available from the corresponding author on reasonable request.

References

[1] Abdulkadir BA, Dennis JO, Bin Abd. Shukur MF, Nasef MME, Usman F, Adam AA, et al. Dielectric study of gel polymer electrolyte based on PVA-K_2CO_3 -SiO_2. IOP Conf Ser Mater Sci Eng. 2021;1092:012066. doi: 10.1088/1757-899x/1092/1/012066.

[2] Mukherjee C, Varghese D, Krishna JS, Boominathan T, Rakeshkumar R, Dineshkumar S, et al. Recent advances in biodegradable polymers – Properties, applications and future prospects. Eur Polym J. 2023;192:112068. doi: 10.1016/j.eurpolymj.2023.112068.

[3] Amalraj J, Lakshmanan P, Amarnath CA, Pyarasani RD, Saravanan C. Biodegradable polymer blend nanocomposites for energy storage application. Polymer blend nanocomposites for energy storage applications. Elsevier Inc; 2023. p. 175–202. doi: 10.1016/B978-0-323-99549-8.00009-1.

[4] Rayung M, Aung MM, Azhar SC, Abdullah LC, Su'ait MS, Ahmad A, et al. Bio-based polymer electrolytes for electrochemical devices: Insight into the ionic conductivity performance. Materials (Basel). 2020;13:838. doi: 10.3390/ma13040838.

[5] Mohanapriya S, Rambabu G, Bhat SD, Raj V. Pectin based nanocomposite membranes as green electrolytes for direct methanol fuel cells. Arab J Chem. 2020;13:2024–40. doi: 10.1016/j.arabjc.2018.03.001.

[6] Tomi R, Daisuke T, Toshihiko K. Characteristics of electric double-layer capacitors based on solid polymer electrolyte composed of sodium polyacrylate. J Phys Conf Ser. 2022;2368:012002. doi: 10.1088/1742-6596/2368/1/012002.

[7] Hadi JM, Aziz SB, Nofal MM, Hussen SA, Hamsan MH, Brza MA, et al. Electrical, dielectric property and electrochemical performances of plasticized silver ion-conducting chitosan-based polymer nanocomposites. Membranes (Basel). 2020;10:151. doi: 10.3390/membranes10070151.

[8] Lage-Rivera S, Ares-Pernas A, Abad MJ. Last developments in polymers for wearable energy storage devices. Int J Energy Res. 2022;46:10475–98. doi: 10.1002/er.7934.

[9] Muralee Gopi CVV, Vinodh R, Sambasivam S, Obaidat IM, Kim HJ. Recent progress of advanced energy storage materials for flexible and wearable supercapacitor: From design and development to applications. J Energy Storage. 2020;27:101035. doi: 10.1016/j.est.2019.101035.
[10] Kraiwattanawong K. A review on the development of a porous carbon-based as modeling materials for electric double layer capacitors. Arab J Chem. 2022;15:103625. doi: 10.1016/j.arabjc.2021.103625.
[11] Sadiq M, Raza MMH, Murtaza T, Zulfequar M, Ali J. Sodium ion-conducting polyvinylpyrrolidone (PVP)/polyvinyl alcohol (PVA) blend electrolyte films. J Electron Mater. 2021;50:403–18. doi: 10.1007/s11664-020-08581-1.
[12] Gautam L, Warkar SG, Ahmad SI, Kant R, Jain M. A review on carboxylic acid cross-linked polyvinyl alcohol: Properties and applications. Polym Eng Sci. 2022;62:225–46. doi: 10.1002/pen.25849.
[13] Sharma S, Sudhakara P, Singh J, Ilyas RA, Asyraf MRM, Razman MR. Critical review of biodegradable and bioactive polymer composites for bone tissue engineering and drug delivery applications. Polymers (Basel). 2021;13:2623. doi: 10.3390/polym13162623.
[14] Huang J, Chen M, Zhou Y, Li Y, Hu Y. Functional characteristics improvement by structural modification of hydroxypropyl methylcellulose modified polyvinyl alcohol films incorporating roselle anthocyanins for shrimp freshness monitoring. Int J Biol Macromol. 2020;162:1250–61. doi: 10.1016/j.ijbiomac.2020.06.156.
[15] Abdulwahid RT, Aziz SB, Kadir MFZ. Insights into ion transport in biodegradable solid polymer blend electrolyte based on FTIR analysis and circuit design. J Phys Chem Solids. 2022;167:110774. doi: 10.1016/j.jpcs.2022.110774.
[16] Abedi-Firoozjah R, Chabook N, Rostami O, Heydari M, Kolahdouz-Nasiri A, Javanmardi F, et al. PVA/starch films: An updated review of their preparation, characterization, and diverse applications in the food industry. Polym Test. 2023;118:107903. doi: 10.1016/j.polymertesting.2022.107903.
[17] Mustafa MF, Ridwan NIM, Hatta FF, Yahya MZA. Effect of dimethyl carbonate plasticizer on ionic conductivity of methyl cellulose-based polymer electrolytes. Malaysian J Anal Sci. 2012;16:283–9.
[18] Teleky B-E, Mitrea L, Plamada D, Nemes SA, Călinoiu, Lavinia-Florina MSP, et al. Development of pectin and poly(vinyl alcohol)-based active packaging enriched with itaconic acid and apple pomace-derived antioxidants. Antioxid Artic. 2022;11:1729. doi: 10.3390/antiox11091729.
[19] Jiménez-Gómez CP, Cecilia JA. Chitosan: A natural biopolymer with a wide and varied range of applications. Molecules. 2020;25:3981. doi: 10.3390/molecules25173981.
[20] Leceta I, Guerrero P, De La Caba K. Functional properties of chitosan-based films. Carbohydr Polym. 2013;93:339–46. doi: 10.1016/j.carbpol.2012.04.031.
[21] Tezotto-Uliana JV, Fargoni GP, Geerdink GM, Kluge RA. Chitosan applications pre- or postharvest prolong raspberry shelf-life quality. Postharvest Biol Technol. 2014;91:72–7. doi: 10.1016/j.postharvbio.2013.12.023.
[22] Sahraei Khosh Gardesh A, Badii F, Hashemi M, Ardakani AY, Maftoonazad N, Gorji AM. Effect of nanochitosan based coating on climacteric behavior and postharvest shelf-life extension of apple cv. Golab Kohanz. LWT. 2016;70:33–40. doi: 10.1016/j.lwt.2016.02.002.
[23] Duran M, Aday MS, Zorba NND, Temizkan R, Büyükcan MB, Caner C. Potential of antimicrobial active packaging "containing natamycin, nisin, pomegranate and grape seed extract in chitosan coating" to extend shelf life of fresh strawberry. Food Bioprod Process. 2016;98:354–63. doi: 10.1016/j.fbp.2016.01.007.
[24] Liu K, Liu J, Li H, Yuan C, Zhong J, Chen Y. Influence of postharvest citric acid and chitosan coating treatment on ripening attributes and expression of cell wall related genes in cherimoya (Annona cherimola Mill.) fruit. Sci Hortic (Amst). 2016;198:1–11. doi: 10.1016/j.scienta.2015.11.008.
[25] Petriccione M, Pasquariello MS, Mastrobuoni F, Zampella L, Di Patre D, Scortichini M. Influence of a chitosan coating on the quality and nutraceutical traits of loquat fruit during postharvest life. Sci Hortic (Amst). 2015;197:287–96. doi: 10.1016/j.scienta.2015.09.051.
[26] Hadi JM, Aziz SB, Saeed SR, Brza MA, Abdulwahid RT, Hamsan MH, et al. Investigation of ion transport parameters and electrochemical performance of plasticized biocompatible chitosan-based proton conducting polymer composite electrolytes. Membranes (Basel). 2020;10:363. doi: 10.3390/membranes10110363.
[27] Shukur MF, Ithnin R, Kadir MFZ. Ionic conductivity and dielectric properties of potato starch-magnesium acetate biopolymer electrolytes: the effect of glycerol and 1-butyl-3-methylimidazolium chloride. Ion (Kiel). 2016;22:1113–23. doi: 10.1007/s11581-015-1627-4.
[28] Chai MN, Isa MIN. Novel proton conducting solid bio-polymer electrolytes based on carboxymethyl cellulose doped with oleic acid and plasticized with glycerol. Sci Rep. 2016;6:27328. doi: 10.1038/srep27328.
[29] Mattos RI, Raphael E, Majid SR, Arof AK, Pawlicka A. Enhancement of electrical conductivity in plasticized chitosan based membranes. Mol Cryst Liq Cryst. 2012;554:150–9. doi: 10.1080/15421406.2012.633862.
[30] Nasef MM, Saidi H, Dahlan KZM. Preparation of composite polymer electrolytes by electron beam-induced grafting: Proton- and lithium ion-conducting membranes. Nucl Instrum Methods Phys Res Sect B Beam Interact Mater At. 2007;265:168–72. doi: 10.1016/j.nimb.2007.08.044.
[31] Biskri ZE, Rached H, Bouchear M, Rached D, Aida MS. A comparative study of structural stability and mechanical and optical properties of fluorapatite ($Ca_5(PO_4)_3F$) and lithium disilicate ($Li_2Si_2O_5$) components forming dental glass–ceramics: First principles study. J Electron Mater. 2016;45:5082–95. doi: 10.1007/s11664-016-4681-4.
[32] Abdulwahid RT, Aziz SB, Kadir MFZ. Environmentally friendly plasticized electrolyte based on chitosan (CS): Potato starch (PS) polymers for EDLC application: Steps toward the greener energy storage devices derived from biopolymers. J Energy Storage. 2023;67:107636. doi: 10.1016/j.est.2023.107636.
[33] Dennis JO, Adam AA, Ali MKM, Soleimani H, Shukur MFBA, Ibnaouf KH, et al. Substantial proton ion conduction in methylcellulose/pectin/ammonium chloride based solid nanocomposite polymer electrolytes: Effect of ZnO nanofiller. Membranes (Basel). 2022;12:706. doi: 10.3390/membranes12070706.
[34] Adam AA, Soleimani H, Shukur MFBA, Dennis JO, Abdulkadir BA, Hassan YM, et al. A new approach to understanding the interaction effect of salt and plasticizer on solid polymer electrolytes using statistical model and artificial intelligence algorithm. J Non Cryst Solids. 2022;587:121597. doi: 10.1016/j.jnoncrysol.2022.121597.
[35] Tripathi M, Tripathi SK. Electrical studies on ionic liquid-based gel polymer electrolyte for its application in EDLCs. Ion (Kiel). 2017;23:2735–46. doi: 10.1007/s11581-017-2051-8.
[36] Abdulwahid RT, Aziz SB, Kadir MFZ. Design of proton conducting solid biopolymer blend electrolytes based on chitosan-potato

starch biopolymers: Deep approaches to structural and ion relaxation dynamics of H^+ ion. J Appl Polym Sci. 2022;139:e52892. doi: 10.1002/app.52892.
[37] Kim KM, Ryu KS, Kang S-G, Chang SH, Chung IJ. The effect of silica addition on the properties of poly((vinylidene fluoride)-co-hexafluoropropylene)-based polymer electrolytes. Macromol Chem Phys. 2001;202:866–72. doi: 10.1002/1521-3935(20010301)202:6<866::aid-macp866>3.3.co;2-3.
[38] Fuzlin AF, Rasali NMJ, Samsudin AS. Effect on ammonium bromide in dielectric behavior based alginate solid biopolymer electrolytes. IOP Conf Ser Mater Sci Eng. 2018;342:012080. doi: 10.1088/1757-899X/342/1/012080.
[39] Aziz SB, Abidin ZHZ. Electrical and morphological analysis of chitosan: AgTf solid electrolyte. Mater Chem Phys. 2014;144:280–6. doi: 10.1016/j.matchemphys.2013.12.029.
[40] Chaurasia SK, Saroj AL, Shalu, Singh VK, Tripathi AK, Gupta AK, et al. Studies on structural, thermal and AC conductivity scaling of PEO-$LiPF_6$ polymer electrolyte with added ionic liquid [$BMIMPF_6$]. AIP Adv. 2015;5:077178. doi: 10.1063/1.4927768.
[41] Tripathi SK, Jain A, Gupta A, Mishra M. Electrical and electrochemical studies on magnesium ion-based polymer gel electrolytes. J Solid State Electrochem. 2012;16:1799–806. doi: 10.1007/s10008-012-1656-0.
[42] Basha SKS, Sundari GS, Kumar KV, Rao MC. Structural and dielectric properties of PVP based composite polymer electrolyte thin films. J Inorg Organomet Polym Mater. 2017;27:455–66. doi: 10.1007/s10904-016-0487-3.
[43] Pradhan DK, Choudhary RNP, Samantaray BK. Studies of dielectric and electrical properties of plasticized polymer nanocomposite electrolytes. Mater Chem Phys. 2009;115:557–61. doi: 10.1016/j.matchemphys.2009.01.008.
[44] Pradhan DK, Choudhary RNP, Samantaray BK. Studies of dielectric relaxation and AC conductivity behavior of plasticized polymer nanocomposite electrolytes. Int J Electrochem Sci. 2008;3:597–608.
[45] Nithya H, Selvasekarapandian S, Arun Kumar D, Sakunthala A, Hema M, Christopherselvin P, et al. Thermal and dielectric studies of polymer electrolyte based on P(ECH-EO). Mater Chem Phys. 2011;126:404–8. doi: 10.1016/j.matchemphys.2010.10.047.
[46] Kulshrestha N, Chatterjee B, Gupta PN. Structural, thermal, electrical, and dielectric properties of synthesized nanocomposite solid polymer electrolytes. High Perform Polym. 2014;26:677–88. doi: 10.1177/0954008314541820.
[47] Agrawal SL, Singh M, Tripathi M, Dwivedi MM, Pandey K. Dielectric relaxation studies on [PEO-SiO_2]: NH4SCN nanocomposite polymer electrolyte films. J Mater Sci. 2009;44:6060–8. doi: 10.1007/s10853-009-3833-9.
[48] Manjunatha H, Damle R, Pravin K, Kumaraswamy GN. Modification in the transport and morphological properties of solid polymer electrolyte system by low-energy ion irradiation. Ion (Kiel). 2018;24:3027–37. doi: 10.1007/s11581-018-2518-2.
[49] Hadi JM, Aziz SB, Mustafa MS, Brza MA, Hamsan MH, Kadir MFZ, et al. Electrochemical impedance study of proton conducting polymer electrolytes based on PVC doped with thiocyanate and plasticized with glycerol. Int J Electrochem Sci. 2020;15:4671–83. doi: 10.20964/2020.05.34.
[50] Subba Reddy CV, Han X, Zhu QY, Mai LQ, Chen W. Dielectric spectroscopy studies on (PVP + PVA) polyblend film. Microelectron Eng. 2006;83:281–5. doi: 10.1016/j.mee.2005.08.010.
[51] Hirankumar G, Mehta N. Effect of incorporation of different plasticizers on structural and ion transport properties of PVA-$LiClO_4$ based electrolytes. Heliyon. 2018;4:e00992. doi: 10.1016/j.heliyon.2018.e00992.
[52] Nicolau A, Nucci AM, Martini EMA, Samios D. Electrical impedance spectroscopy of epoxy systems II: Molar fraction variation, resistivity, capacitance and relaxation processes of 1,4-butanediol diglycidyl ether/succinic anhydride and triethylamine as initiator. Eur Polym J. 2007;43:2708–17. doi: 10.1016/j.eurpolymj.2007.03.018.
[53] Wang W, Alexandridis P. Composite polymer electrolytes: Nanoparticles affect structure and properties. Polymers. 2016;8:387. doi: 10.3390/polym8110387.
[54] Marzantowicz M, Dygas JR, Krok F, Florjańczyk Z, Zygadło-Monikowska E. Conductivity and dielectric properties of polymer electrolytes PEO:$LiN(CF_3SO_2)_2$ near glass transition. J Non Cryst Solids. 2007;353:4467–73. doi: 10.1016/j.jnoncrysol.2007.04.046.
[55] Jiang H, Hong L, Venkatasubramanian N, Grant JT, Eyink K, Wiacek K, et al. The relationship between chemical structure and dielectric properties of plasma-enhanced chemical vapor deposited polymer thin films. Thin Solid Films. 2007;515:3513–20. doi: 10.1016/j.tsf.2006.10.126.
[56] Rafi NSM, Abidin SZZ, Majid SR, Zakaria R. Preparation of agarose-based biopolymer electrolytes containing calcium thiocyanate: Electrical and electrochemical properties. Int J Electrochem Sci. 2022;17:220713. doi: 10.20964/2022.07.21.
[57] Vahini M, Muthuvinayagam M, Isa MIN. Preparation and characterization of biopolymer electrolytes based on pectin and $NaNO_3$ for battery applications. Polym Sci - Ser A. 2019;61:823–31. doi: 10.1134/S0965545X19060129.
[58] Aziz SB, Brevik I, Hamsan MH, Brza MA, Nofal MM, Abdullah AM, et al. Compatible solid polymer electrolyte based on methyl cellulose for energy storage application: Structural, electrical, and electrochemical properties. Polymers (Basel). 2020;12:2257. doi: 10.3390/polym12102257.
[59] Abdulwahid RT, Aziz SB, Kadir MFZ. Replacing synthetic polymer electrolytes in energy storage with flexible biodegradable alternatives: sustainable green biopolymer blend electrolyte for supercapacitor device. Mater Today Sustain. 2023;23:100472. doi: 10.1016/j.mtsust.2023.100472.
[60] Abbas Adam A, Soleimani H, Muhammad MF, Ojur Dennis J, Abubakar Abdulkadir B, Mudassir Hassan Y, et al. Structural behavior and ion dynamics of methylcellulose/tri-potassium phosphate-based solid biopolymeric electrolytes. Mol Cryst Liq Cryst. 2022;759:29–34.
[61] Teo LP, Buraidah MH, Arof AK. Development on solid polymer electrolytes for electrochemical devices. Molecules. 2021;26:6499. doi: 10.3390/molecules26216499.
[62] Ibrahim S, Ahmad A, Mohamed NS. Characterization of novel castor oil-based polyurethane polymer electrolytes. Polymers (Basel). 2015;7:747–59. doi: 10.3390/polym7040747.
[63] Irfan M, Manjunath A, Mahesh SS, Somashekar R, Demappa T. Influence of NaF salt doping on electrical and optical properties of PVA/PVP polymer blend electrolyte films for battery application. J Mater Sci Mater Electron. 2021;32:5520–37. doi: 10.1007/s10854-021-05274-1.
[64] Muchakayala R, Song S, Wang J, Fan Y, Bengeppagari M, Chen J, et al. Development and supercapacitor application of ionic liquid-incorporated gel polymer electrolyte films. J Ind Eng Chem. 2018;59:79–89. doi: 10.1016/j.jiec.2017.10.009.
[65] Petnikota S, Chua R, Zhou Y, Edison E, Srinivasan M. Amorphous vanadium oxide thin films as stable performing cathodes of lithium and sodium-ion batteries. Nanoscale Res Lett. 2018;13:363. doi: 10.1186/s11671-018-2766-0.

[66] Pal B, Yang S, Ramesh S, Thangadurai V, Jose R. Electrolyte selection for supercapacitive devices: A critical review. Nanoscale Adv. 2019;1:3807–35. doi: 10.1039/c9na00374f.
[67] Nadiah NS, Omar FS, Numan A, Mahipal YK, Ramesh S, Ramesh K. Influence of acrylic acid on ethylene carbonate/dimethyl carbonate based liquid electrolyte and its supercapacitor application. Int J Hydrog Energy. 2017;42:30683–90. doi: 10.1016/j.ijhydene.2017.10.140.
[68] Ngai KS, Ramesh S, Ramesh K, Juan JC. A review of polymer electrolytes: fundamental, approaches and applications. Ion (Kiel). 2016;22:1259–79. doi: 10.1007/s11581-016-1756-4.
[69] Wojciechowski J, Kolanowski Ł, Bund A, Lota G. The influence of current collector corrosion on the performance of electrochemical capacitors. J Power Sources. 2017;368:18–29. doi: 10.1016/j.jpowsour.2017.09.069.
[70] Hamsan MH, Shukur MF, Kadir MFZ. NH_4NO_3 as charge carrier contributor in glycerolized potato starch-methyl cellulose blend-based polymer electrolyte and the application in electrochemical double-layer capacitor. Ion (Kiel). 2017;23:3429–53. doi: 10.1007/s11581-017-2155-1.
[71] Winie T, Jamal A, Saaid FI, Tseng TY. Hexanoyl chitosan/ENR25 blend polymer electrolyte system for electrical double layer capacitor. Polym Adv Technol. 2019;30:726–35. doi: 10.1002/pat.4510.
[72] Yassine M, Fabris D. Performance of commercially available supercapacitors. Energies. 2017;10:1340. doi: 10.3390/en10091340.